High-efficiency Ultrafast Optical-to-Electrical Converters Based on InAs Nanowire-Plasmonic Arrays

DINGKUN REN,[1,†,*] ZIXUAN RONG,[1,†] HYUNSEOK KIM,[1,*] DENIZ TURAN,[1] DIANA L. HUFFAKER[1,2,3]

[1]Department of Electrical and Computer Engineering, University of California, Los Angeles, Los Angeles, California 90095, United States
[2]California NanoSystems Institute, University of California, Los Angeles, Los Angeles, California 90095, United States
[3]School of Physics and Astronomy, Cardiff University, Cardiff, Wales CF24 3AA, United Kingdom
†These authors contributed equally to this Letter.
*Corresponding author: dingkun.ren@ucla.edu and hyunseokkim@ucla.edu

There has been a growing interest in developing high-efficiency ultrafast optical-to-electrical converters for advanced imaging and sensing applications. Here, we propose a three-dimensional (3D) plasmonic platform based on InAs nanowire arrays with self-assembled gold gratings, which converts telecom-wavelength (1550 nm) optical beam to sub-picosecond current pulses with a quantum efficiency up to 18.3%, while operating in photovoltaic mode, i.e., at zero bias. Using a comprehensive 3D photoresponse model, we reveal that the incident photons form tightly confined fields near the gratings at nanowire tips, and thus majority of the photogenerated carriers are efficiently routed to the metal within a few tens of nanometers distance, resulting in ultrafast current pulses. In addition, we show that the amplitude of current pulses is robust to the nanowire surface quality and can be effectively tuned by varying the doping levels in nanowires. This work paves a way to realizing a low-power, highly compact, and low-cost device scheme for ultrafast pulse generation. © 2019 Optical Society of America

OCIS codes: (160.4236) Nanomaterials; (250.0040) Detectors; (040.3060) Infrared.

http://dx.doi.org/10.1364/OL.99.099999

Ultrashort electrical pulses are utilized as a building block for diverse applications, including spectroscopy, imaging, sensing, and high-frequency technologies [1]. One of the widely used approaches to generate ultrashort pulses is utilizing optical-to-electrical conversion, which transforms optical pulses to electrical pulses [2-5]. To date, planar plasmonic optical-to-electrical converters, wherein photogenerated carriers are collected as current signals through metal contacts by photoconduction, have demonstrated promising performance and have been one of the most commonly used techniques for generating sub-picosecond current pulses [6-9]. In this approach, plasmonic contact electrodes concentrate a large portion of the incident optical pump beam in close proximity to the contact electrodes. By reducing the average transport path length of the photogenerated carriers from the contact electrodes, a larger number of carriers drifts to the contacts within a sub-picosecond time-scale. However, "slow" carriers (typically further than ~100 nm from contacts) still exist and optical confinement is not fully optimized. As a result, a bias voltage is typically required to generate strong electric field to quickly drift these slow carriers, while this leads to high dark current and thermal breakdown.

To overcome this issue, we present a device platform based on InAs nanowire-plasmonic photoabsorber arrays monolithically integrated on Si or InP substrate, which can operate in photovoltaic mode (i.e. at zero bias). It converts telecom-wavelength (1550 nm) optical pulses to sub-picosecond current pulses with a quantum efficiency up to 18.3%. In this transformative converter, three-dimensional (3D) nanowire-plasmonic photoabsorbers are the key enablers, which almost completely eliminates the generation of 'slow' photocarriers. In specific, by utilizing metal nanostructures as 3D plasmonic gratings self-assembled to InAs nanowire arrays, the majority of the incident photons are confined within nanoscale distances from the metal contacts [10-12], and thus the majority of the photocarriers can be quickly collected by metal gratings and contribute to a rapid current response [13].

The architecture of our 3D optical-to-electrical converter is shown in Fig. 1(a). Vertical InAs nanowire-plasmonic photoabsorber arrays are integrated with self-assembled gold gratings. Benzocyclobutene (BCB) is considered as a dielectric spacer to control the exposed height of nanowires [10-12]. We note that monolithic integration of InAs nanowires on Si and InP substrates has been demonstrated by selective-area epitaxy using metal-organic chemical vapor deposition (MOCVD) [14-16], and self-assembly of metal gratings has been achieved by angled

deposition of metal, which ensures the feasibility of our approach [10-12]. By using the nanowires themselves as shadow masks, gold can be deposited on the nanowire-bearing surface to create an array of airholes, i.e., a plasmonic grating. In order to show the device performance, we take a simulation approach to compute the output current pulses and quantum efficiencies using a 3D photoresponse model [17,18]. Note that our model can fully capture 3D features of nanowires and carrier dynamics to properly compute the photoresponse. This cannot be done by using either 2D or 1D model. Therefore, analytical solutions are of limited applicability, and it is necessary to use a 3D computational model. In this study, we first maximize the optical absorption of 3D photoabsorbers by tuning the geometric dimensions. Then, we consider the nanowire doping concentration to optimize the output current pulses. Finally, we investigate the impact of nanowire surface quality on the amplitude of current pulses.
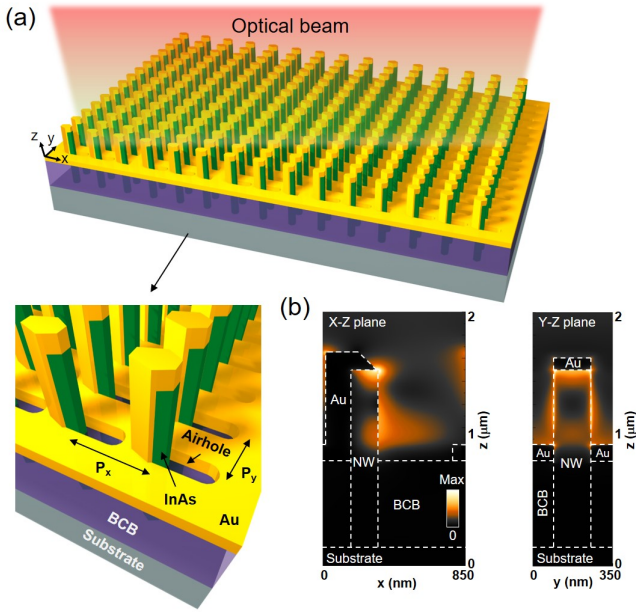

Fig. 1. (a) Schematic diagram of optical-to-electrical converter based on InAs nanowire-plasmonic photoabsorber array. P_x and P_y represent the nanowire array pitches along x and y directions, respectively. (b) Electric-field profile ($|E|$) of the structure at a 1550 nm pump wavelength.

Optical absorption was simulated by Lumerical finite-difference time-domain (FDTD). A square unit cell with a single InAs nanowire-plasmonic photoabsorber with a periodic boundary condition was used in the simulations. The total number of nanowires in each photoabsorber array can be made large (on the order of thousands), and hence the error associated with using a periodic boundary condition, which assumes infinite number of nanowires, is negligible. As shown in the typical electric field profile of a unit cell in Fig. 1(b), the field is tightly confined in nanowires near metal gratings, which is the major advantage of our approach compared with planar optical-to-electrical converters. To achieve the optimized optical absorption at a 1550 nm pump wavelength, we finely tuned several geometric parameters: (1) the nanowire diameter D_{NW}, (2) the exposed nanowire height H_{Ex}, (3) the nanowire array pitch P_x and P_y, and (4) the thickness of the gold layer T_{Au}. The length of the airhole L_{Hole} was kept fixed at 560 nm. Note that the periodicity of the airhole

array can support surface plasmon resonances, similar to the mechanism of typical planar plasmonic gratings [19]. Further enhancement of resonances can be achieved by finely tuning the geometry of those subwavelength airholes. Additionally, we also varied (5) the incident angle of the optical pump beam θ, and (6) the polarization of the optical pump beam. The simulation results show photo-absorption of more than 40% can be achieved at 1550 nm with the dimensions shown in Fig. 2(a) and at a pump incident angle of 30° and polarization along x-direction (i.e., electric field along x-direction). Fig. 2(b) and 2(c) show the impact of four individual geometric parameters and two individual incidence properties on optical absorption. The excited surface plasmon waves induce most of the field to be tightly confined at the exposed nanowire tips, as shown in the electric-field profiles in Fig. 1(b), and thus the effect of substrate materials on the optical mode is negligible. Additionally, since the nanowire-based platform operates in photovoltaic mode, the electrical performance is entirely dependent on the nanowire segments, not the substrate.
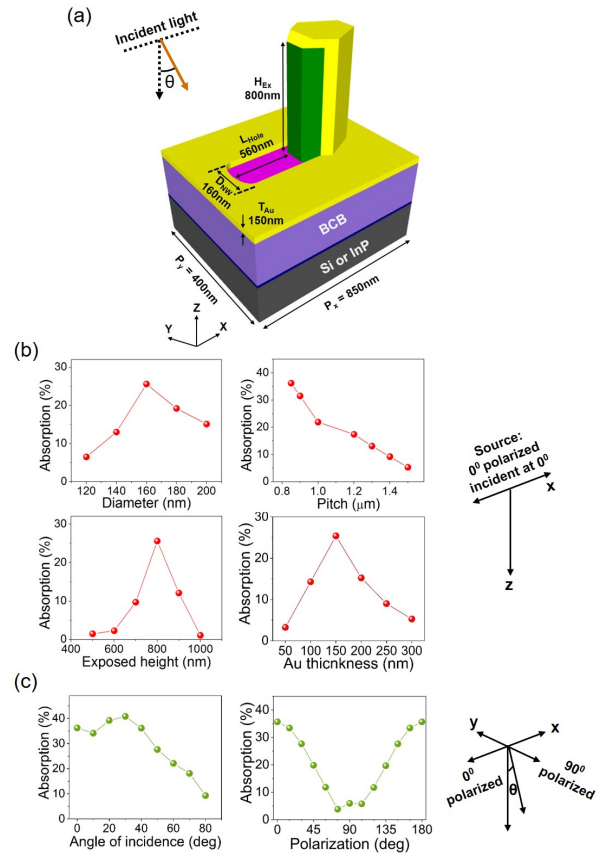

Fig. 2. (a) Optimized dimensions for an InAs nanowire photoabsorber at 1550 nm optical wavelength. (b) Optical absorption as a function of photoabsorber geometric parameters. The geometric parameters include the nanowire diameter D_{NW}, exposed nanowire height H_{Ex}, pitch of the array P_x, and Au thickness T_{Au}. (c) Optical absorption as a function of incidence properties including angle of the optical pump beam θ and polarization.

Based on these optical field profiles calculated by FDTD, we convert the field intensity inside a single nanowire-plasmonic photoabsorber to a 3D optical generation rate profile using an electrical model (Sentaurus TCAD), as shown in Fig. 3(a). To compute the photoresponse, we assumed that the optical pump

beam is a femtosecond laser with a pulse width of 50 fs FWHM and an average power of 16 μW (peak power of 4.5 W), and a beam diameter of 15 μm (illuminating ~500 nanowires). These parameters are based on a femtosecond laser setup at the 1550 nm that generates optical pulses with 50 fs pulse width and 50 MHz repetition rate. In the simulations, we set the peak of laser pulse at 100 fs. Here we assume that the size of the nanowire-plasmonic array is 15×15 μm^2 and keep the surface recombination velocity fixed at 1×10^4 cm/s, while the effect of the surface recombination velocity will be discussed in the later section. Fig. 4(b) shows the induced photocurrent in *n*-type InAs nanowires with the doping concentration of 1×10^{18} cm^{-3}, where this value is adopted based on the reports that unintentionally doped InAs grown by MOCVD is *n*-type [11,20]. The current pulse clearly shows that the nanoscale distance for the photo-generated carriers to reach the metal contacts offers an ultrafast photocurrent response with less than 100 fs FWHM. Since no bias is applied to the photoabsorbers, the dark current is zero. To understand the carrier dynamics in those nanoscale photoabsorbers, we visualized the 3D spatial carrier distribution at different points of time in photovoltaic mode. Fig. 3(c) shows the hole (minority carrier) density in a cross-section at 45 fs, 95 fs, 140 fs, 230 fs, and 1000 fs, respectively. The photocurrent reaches its maximum at ~140 fs, which is ~40 fs after the laser peak reaches its peak. Then it decreases rapidly, reaching 10 % of the maximum value in ~100 fs.
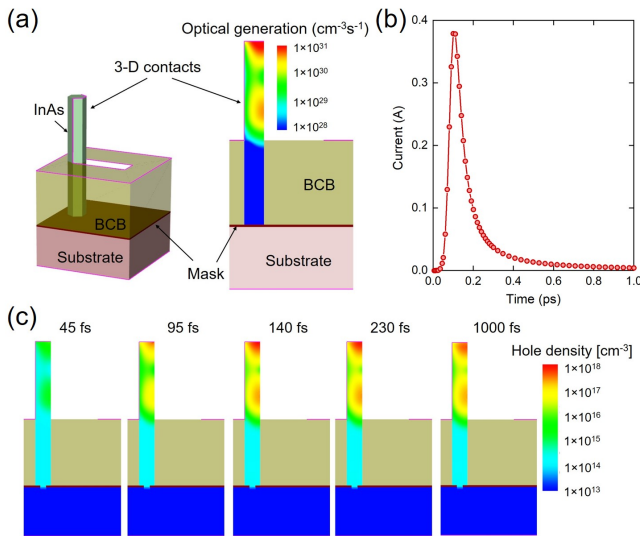

Fig. 3. (a) The profile of the optical generation rate inside the nanowire photoabsorber in response to a pump beam. (b) The induced photocurrent for *n*-type nanowires with a doping level of 1×10^{18} cm^{-3}. The size of nanowire-plasmonic array is 15×15 μm^2. (c) The cross-sectional spatial distribution of holes (minority carriers) as a function of time: 45 fs, 95 fs, 140 fs, 230 fs, and 1000 fs.

Next, we studied the effect of nanowire doping concentration on the photoresponse of nanowire-plasmonic converters. To consider realistic cases, the mobility of InAs nanowires is adjusted according to the doping concentration in the transient simulation model. As shown in Fig. 4, the peak of induced photocurrent can be increased significantly by using higher doping levels, in the range of 1×10^{16} cm^{-3} to 1×10^{18} cm^{-3} for both *n*-type and *p*-type InAs nanowires. This is because a higher doping level results in a lower Schottky barrier, leading to a more rapid acceleration of carriers

toward the 3D metal contacts. Additionally, we note that at the same doping concertation, *p*-type InAs nanowires offer higher photocurrent than *n*-type ones. This can be attributed to the difference of InAs carrier mobilities between electrons and holes. In specific, it is well known that the electron mobility of InAs is much higher than the hole mobility, and when *p*-type InAs nanowires are employed as photoabsorbers, electrons are the minority carriers and contribute to the major portion of photocurrent. Thus, photogenerated carriers can be more efficiently collected by the metal contacts.

To calculate the quantum efficiency of the converters, we integrated the current shown in Fig. 4 and divided it by the incident power of 16 μW. Table 1 lists the calculated quantum efficiency as a function of doping concentration. The highest estimated quantum efficiencies are 11.54% and 18.36% for *n*-type and *p*-type photoabsorbers, respectively, with a doping concentration of 1×10^{18} cm^{-3}. As one can expect from the trend of peak current in Fig. 4, higher doping level contributes to higher quantum efficiency. We note that it is possible to achieve even higher quantum efficiency by employing InAs nanowires with the doping concentration higher than 1×10^{18} cm^{-3}, but it is challenging to achieve such a high doping level by selective-area nanowire epitaxy. An alternative approach for higher efficiency is to introduce a *p-n* junction within nanowires, by which the carriers are quickly swept to the metal contacts by intrinsic electric fields in the *p-n* junction. This can be realized by growing nanowires as a 'core-shell' structure with *p*-type core and *n*-shell, where the growth of such structures has been already demonstrated.
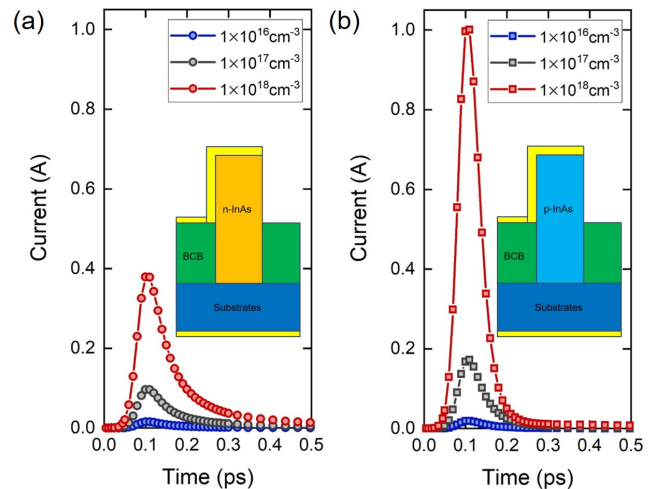

Fig. 4. The induced photocurrent for *n*-type and *p*-type nanowires with doping levels ranging from 1×10^{16} cm^{-3} to 1×10^{18} cm^{-3}. The size of nanowire-plasmonic array is 15×15 μm^2.

Table 1. Optical-to-Electrical Quantum Efficiency

Doping concentration	*n*-type	*p*-type
1×10^{16}	0.49%	0.54%
1×10^{17}	3.21%	3.77%
1×10^{18}	11.54%	18.36%

Finally, we took the nanowire surface quality into account and analyzed the impact of surface recombination velocity on the induced photocurrent. Nonradiative recombination centers on surfaces, which are also called as surface states, are caused by a sudden termination of crystal lattices, and can result in higher noise and lower photocurrent. Due to the large surface-to-volume

ratio in nanowires, the performance of nanowire-based devices is often dominated by nonradiative recombination on their surfaces [21,22]. Thus, it is crucial to consider the effect of nanowire surfaces on the device performance. Here, we kept the nanowire geometric parameters unchanged (same as those used in Fig. 4) and calculated the peak current under different surface recombination velocities ranging from 1×10^2 cm/s to 1×10^6 cm/s for both n-type and p-type nanowires, as shown in Fig. 5. Typical surface recombination velocities reported for InAs are on the order of 10^3–10^4 cm/s, both for thin films and nanowires [12,23,24], and hence the range of surface recombination velocities considered here well covers empirical values. Interestingly, we observe that the peak current intensity is almost invariant from 1×10^2 cm/s up to 1×10^5 cm/s, for both n-type and p-type nanowires. On other words, the nonradiative recombination on nanowire surfaces has negligible effect on the output electrical signals in the proposed device, unlike typical nanowire-based optoelectronic devices whose performances are significantly affected by the surface quality. This is because the period required for most of the photogenerated carriers to reach metal is on the order of sub-picoseconds in the proposed scheme, which is much shorter than the nonradiative lifetime at the surface. As a result, effective surface passivation of nanowires, which is a stringent requirement for many nanowire-based optoelectronic devices, is not necessary in the proposed optical-to-electrical converters.
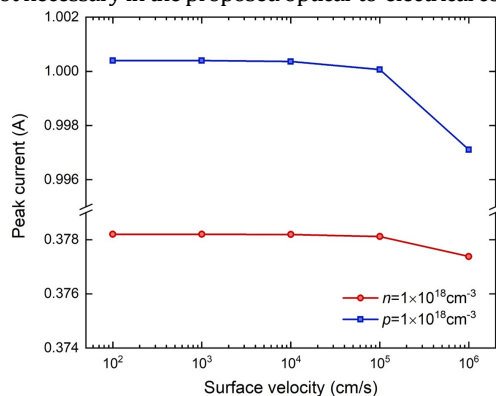

Fig. 5. Peak intensity of photogenerated current pulses as a function of surface recombination velocity of InAs nanowires. The doping concentration is fixed at 1×10^{18} cm^{-3}.

In summary, we showed the feasibility of optical-to-electrical converters based on nanowire-plasmonic photoabsorber arrays to generate ultrafast sub-picosecond current pulses with a quantum efficiency up to 18.3 %. This device platform can operate in photovoltaic mode (i.e., bias-free) with zero dark current. By combining 3D optical FDTD simulation and 3D electrical TCAD modeling, we optimized the geometric and material properties of proposed nanostructures. The result showed that the FWHM of the current pulses is below 100 fs. In addition, we observed that the intensity of current pulses is strongly affected by the nanowire doping concentration, which provides an extra tuning capability for the device design. Last but not least, we showed that the induced current is not sensitive to the nanowire surface quality, meaning that the design rule can be alleviated. This study paves a way to achieving highly efficient, fully integrated and highly compact optical-to-electrical converters for applications in imaging and sensing.

References

1. D. G. Rowe, Nat. Photonics **1**, 75 (2007).
2. D. H. Auston, K. P. Cheung, and P. R. Smith, Appl. Phys. Lett. **45**, 284 (1984).
3. Z. D. Taylor, E. R. Brown, and J. E. Bjarnason, Opt. Lett. **31**, 1729 (2006).
4. P. C. Upadhya, W. Fan, A. Burnett, J. Cunningham, A. G. Davies, E. H. Linfield, J. Lloyd-Hughes, E. CastroCamus, M. B. Johnston, and H. Beere, Opt. Lett. **32**, 2297 (2007).
5. H. Roehle, R. J. B. Dietz, H. J. Hensel, J. Böttcher, H. Künzel, D. Stanze, M. Schell, and B. Sartorius, Opt. Express **18**, 2296 (2010).
6. C. W. Berry, N. Wang, M. R. Hashemi, M. Unlu, and M. Jarrahi, Nat. Commun. **4**, 1622 (2013).
7. C. W. Berry, M. R. Hashemi, S. Preu, H. Lu, A. C. Gossard, and M. Jarrahi, Opt. Lett. **39**, 4522 (2014).
8. M. Jarrahi, IEEE Trans. Terahertz Sci. Technol. **5**, 391 (2015).
9. N. T. Yardimci and M. Jarrahi, Appl. Phys. Lett. **109**, 191103 (2016).
10. P. Senanayake, C.-H. Hung, J. Shapiro, A. Lin, B. Liang, B. S. Williams, and D. L. Huffaker, Nano Lett. **11**, 5279 (2011).
11. D. Ren, X. Meng, Z. Rong, C. Minh, A. C. Farrell, S. Somasundaram, K. M. Azizur-Rahman, B. S. Williams, and D. L. Huffaker, Nano Lett. **18**, 7901 (2018).
12. D. Ren, K. M. Azizur-Rahman, Z. Rong, B.-C. Juang, S. Somasundaram, M. Shahili, A. C. Farrell, B. S. Williams, and D. L. Huffaker, Nano Lett. **19**, 2793 (2019).
13. A. C. Farrell, X. Meng, D. Ren, H. Kim, P. Senanayake, N. Y. Hseih, Z. Rong, T.-Y. Chang, K. M. Azizur-Rahman, and D. L. Huffaker, Nano Lett. **19**, 582 (2019).
14. K. Tomioka, J. Motohisa, S. Hara, and T. Fukui, Nano Lett. **8**, 3475 (2008).
15. H. Kim, A. C. Farrell, P. Senanayake, W.-J. Lee, and D.L. Huffaker, Nano Lett. **16**, 1833 (2016).
16. D. Ren, A. C. Farrell, B. S. Williams, and D. L. Huffaker, Nanoscale **9**, 8220 (2017).
17. D. Ren, A. C. Scofield, A. C. Farrell, Z. Rong, M. A. Haddad, R. B. Laghumavarapu, B. Liang, and D. L. Huffaker, Nanoscale **10**, 792 (2018).
18. D. Ren, Z. Rong, K. M. Azizur-Rahman, S. Somasundaram, M. Shahili, and D. L. Huffaker, Nanotechnology. **30**, 044002 (2019).
19. S. C. Lee, S. Krishna, and S. R. J. Brueck, Opt. Express **17**, 23160 (2009).
20. A. Lin, J. N. Shapiro, A. C. Scofield, B. L. Liang, and D. L. Huffaker, Appl. Phys. Lett. **102**, 053115 (2013).
21. J. A. Alexander-Webber, C. K. Groschner, A. A. Sagade, G. Tainter, M. F. Gonzalez-Zalba, R. Di Pietro, J. Wong-Leung, H. H. Tan, C. Jagadish, S. Hofmann, and H. J. Joyce, ACS Appl. Mater. Interfaces **9**, 43993 (2017).
22. D. Ren, Z. Rong, S. Somasundaram, K. M. Azizur-Rahman, B. Liang, and D. L. Huffaker, Nanotechnology **29**, 504003 (2018).
23. J. V. Li, S. L. Chuang, E. Aifer, and E. M. Jackson, Appl. Phys. Lett. **90**, 223503 (2007).
24. H. J. Joyce, C. J. Docherty, Q. Gao, H. H. Tan, C. Jagadish, J. Lloyd-Hughes, L. M. Herz, and M. B. Johnston, Nanotechnology **24**, 214006 (2013).

References for Review

1. D. G. Rowe, "Terahertz takes to the stage," Nat. Photonics **1**, 75 (2007).

2. D. H. Auston, K. P. Cheung, and P. R. Smith, "Picosecond photocoducting Hertzian dipoles," Appl. Phys. Lett. **45**, 284 (1984).

3. Z. D. Taylor, E. R. Brown, and J. E. Bjarnason, "Resonant-optical-cavity photoconductive switch with 0.5% conversion efficiency and 1.0W peak power," Opt. Lett. **31**, 1729 (2006).

4. P. C. Upadhya, W. Fan, A. Burnett, J. Cunningham, A. G. Davies, E. H. Linfield, J. Lloyd-Hughes, E. CastroCamus, M. B. Johnston, and H. Beere, "Excitation-density-dependent generation of broadband terahertz radiation in an asymmetrically excited photoconductive antenna," Opt. Lett. **32**, 2297 (2007).

5. H. Roehle, R. J. B. Dietz, H. J. Hensel, J. Böttcher, H. Künzel, D. Stanze, M. Schell, and B. Sartorius, "Next generation 1.5 μm terahertz antennas: mesa-structuring of InGaAs/InAlAs photoconductive layers," Opt. Express **18**, 2296 (2010).

6. C. W. Berry, N. Wang, M. R. Hashemi, M. Unlu, and M. Jarrahi, "Significant performance enhancement in photoconductive terahertz optoelectronics by incorporating plasmonic contact electrodes," Nat. Commun. **4**, 1622 (2013).

7. C. W. Berry, M. R. Hashemi, S. Preu, H. Lu, A. C. Gossard, and M. Jarrahi, "Plasmonics enhanced photomixing for generating continuous-wave frequency-tunable terahertz radiation," Opt. Lett. **39**, 4522 (2014).

8. M. Jarrahi, "Advanced photoconductive terahertz optoelectronics based on nano-antennas and nanoplasmonic light concentrators," IEEE Trans. Terahertz Sci. Technol. **5**, 391 (2015).

9. N. T. Yardimci and M. Jarrahi, "High power telecommunication-compatible photoconductive terahertz emitters based on plasmonic nano-antenna arrays," Appl. Phys. Lett. **109**, 191103 (2016).

10. P. Senanayake, C.-H. Hung, J. Shapiro, A. Lin, B. Liang, B. S. Williams, and D. L. Huffaker, "Surface plasmon-enhanced nanopillar photodetectors" Nano Lett. **11**, 5279 (2011).

11. D. Ren, X. Meng, Z. Rong, C. Minh, A. C. Farrell, S. Somasundaram, K. M. Azizur-Rahman, B. S. Williams, and D. L. Huffaker, "Uncooled photodetector at short-wavelength infrared using InAs nanowire photoabsorbers on InP with p-n heterojunctions," Nano Lett. **18**, 7901 (2018).

12. D. Ren, K. M. Azizur-Rahman, Z. Rong, B.-C. Juang, S. Somasundaram, M. Shahili, A. C. Farrell, B. S. Williams, and D. L. Huffaker, "Room-temperature mid-wavelength infrared InAsSb nanowire photodetector arrays with Al2O3 passivation," Nano Lett. **19**, 2793 (2019).

13. A. C. Farrell, X. Meng, D. Ren, H. Kim, P. Senanayake, N. Y. Hseih, Z. Rong, T.-Y. Chang, K. M. Azizur-Rahman, and D. L. Huffaker, "InGaAs-GaAs nanowire avalanche photodiodes toward single photon detection in free-running mode," Nano Lett. **19**, 582 (2019).

14. K. Tomioka, J. Motohisa, S. Hara, and T. Fukui, "Control of InAs nanowire growth directions on Si," Nano Lett. **8**, 3475 (2008).

15. H. Kim, A. C. Farrell, P. Senanayake, W.-J. Lee, and D.L. Huffaker, "Monolithically integrated InGaAs nanowires on 3D structured silicon-on-insulator as a new platform for full optical links," Nano Lett. **16**, 1833 (2016).

16. D. Ren, A. C. Farrell, B. S. Williams, and D. L. Huffaker, "Seeding layer assisted selective-area growth of As-rich InAsP nanowires on InP substrates," Nanoscale **9**, 8220 (2017).

17. D. Ren, A. C. Scofield, A. C. Farrell, Z. Rong, M. A. Haddad, R. B. Laghumavarapu, B. Liang, and D. L. Huffaker, "Exploring time-resolved photoluminescence for nanowires using a three-dimensional computational transient model," Nanoscale **10**, 792 (2018).

18. D. Ren, Z. Rong, K. M. Azizur-Rahman, S. Somasundaram, M. Shahili, and D. L. Huffaker, "Feasibility of achieving high detectivity at short- and mid-wavelength infrared using nanowire photodetectors with p-n heterojunctions," Nanotechnology. **30**, 044002 (2019).

19. S. C. Lee, S. Krishna, and S. R. J. Brueck, "Quantum dot infrared photodetector enhanced by surface plasma wave excitation," Opt. Express **17**, 23160 (2009).

20. A. Lin, J. N. Shapiro, A. C. Scofield, B. L. Liang, and D. L. Huffaker, "Enhanced InAs nanopillar electrical transport by in-situ passivation," Appl. Phys. Lett. **102**, 053115 (2013).

21. J. A. Alexander-Webber, C. K. Groschner, A. A. Sagade, G. Tainter, M. F. Gonzalez-Zalba, R. Di Pietro, J. Wong-Leung, H. H. Tan, C. Jagadish, S. Hofmann, and H. J. Joyce, "Engineering the photoresponse of InAs nanowires," ACS Appl. Mater. Interfaces **9**, 43993 (2017).

22. D. Ren, Z. Rong, S. Somasundaram, K. M. Azizur-Rahman, B. Liang, and D. L. Huffaker, "A three-dimensional insight into correlation between carrier lifetime and surface recombination velocity for nanowires," Nanotechnology **29**, 504003 (2018).

23. J. V. Li, S. L. Chuang, E. Aifer, and E. M. Jackson, "Surface recombination velocity reduction in type-II InAs/GaSb superlattice photodiodes due to ammonium sulfide passivation," Appl. Phys. Lett. **90**, 223503 (2007).

24. H. J. Joyce, C. J. Docherty, Q. Gao, H. H. Tan, C. Jagadish, J. Lloyd-Hughes, L. M. Herz, and M. B. Johnston, "Electronic properties of GaAs, InAs and InP nanowires studied by terahertz spectroscopy," Nanotechnology **24**, 214006 (2013).